

## Key Points:

- Cold air outbreak (CAO) air masses experience average radiative cooling rates but reside in the Arctic for an exceptionally long time
- Tropopause polar vortices (TPVs) gather cold air masses in the Arctic and contribute to intense CAOs when they approach Fram Strait
- The most intense CAOs are more often related to TPVs (40% of the top 40 events) than weaker ones (20% of the top 60 to top 100 events)

## Correspondence to:

L. Papritz,  
lukas.papritz@env.ethz.ch

## Citation:

Papritz, L., Rouges, E., Aemisegger, F., & Wernli, H. (2019). On the thermodynamic preconditioning of Arctic air masses and the role of tropopause polar vortices for cold air outbreaks from Fram Strait. *Journal of Geophysical Research: Atmospheres*, 124, 11,033–11,050. <https://doi.org/10.1029/2019JD030570>

Received 3 MAR 2019

Accepted 14 SEP 2019

Accepted article online 11 OCT 2019

Published online 5 NOV 2019

## On the Thermodynamic Preconditioning of Arctic Air Masses and the Role of Tropopause Polar Vortices for Cold Air Outbreaks From Fram Strait

Lukas Papritz<sup>1</sup> , Emmanuel Rouges<sup>1,2</sup>, Franziska Aemisegger<sup>1</sup> , and Heini Wernli<sup>1</sup> 

<sup>1</sup>Institute for Atmospheric and Climate Science, ETH Zürich, Zürich, Switzerland, <sup>2</sup>now at European Centre for Medium-Range Weather Forecasts, Reading, UK

**Abstract** Fram Strait is a hot spot of Arctic cold air outbreaks (CAOs), which typically occur within the northerly flow associated with a strong low tropospheric east-west pressure gradient between Svalbard and Greenland. This study investigates the processes in the inner Arctic that thermodynamically precondition air masses associated with CAOs south of Fram Strait where they lead to negative potential temperature anomalies often in excess of 15 K. Kinematic backward trajectories from Fram Strait are used to quantify the Arctic residence time and to analyze the thermodynamic evolution of these air masses. Additionally, the study explores the importance of cyclonic tropopause polar vortices (TPVs) for CAO formation south of Fram Strait. Results from a detailed case study and the climatological analysis of the 100 most intense CAOs from Fram Strait in the ERA-Interim period reveal that (i) air masses that cause CAOs (CAO air masses) reside longer in the inner Arctic compared to those that do not (NO-CAO air masses), and they originate from climatologically colder regions; (ii) the 10-day accumulated cooling is very similar for CAO and NO-CAO air masses indicating that the transport history and northerly origin of the air masses is more decisive for the formation of an intense negative temperature anomaly south of Fram Strait than an enhanced inner Arctic diabatic cooling; (iii) 40% (29%) of the top 40 (100) CAOs are related to a TPV in the vicinity of Fram Strait; (iv) TPVs confine anomalously cold air masses within their associated low tropospheric cold dome leading to enhanced accumulated radiative cooling.

### 1. Introduction

Fram Strait, the passage between Greenland and Svalbard at about 80°N, is an important gateway for the exchange of mass and energy between the northeastern North Atlantic and the inner Arctic, here defined as the basin of the Arctic Ocean (cf. Figure 1 for location names). Especially intense meridional winds over Fram Strait lead to exchange processes that are of key importance for the Arctic climate system. For instance, northerly winds drive the export of sea ice from the Arctic basin into the Greenland Sea and the strength and direction of these winds account for most of the day-to-day variability of the ice export (Jahnke-Bornemann & Brümmer, 2009; Tsukernik et al., 2009). During winter such northerly winds also advect very cold air masses from the inner Arctic over the comparatively warm waters of the Nordic Seas, giving rise to marine cold air outbreaks (CAOs).

Due to the temperature deficit of CAO air masses with respect to the sea surface temperature (SST), intense upward fluxes of sensible heat ensue (e.g., Brümmer, 1997; Renfrew & Moore, 1999; Wacker et al., 2005). Furthermore, as a result of their initial dryness, the rapid warming by sensible heat fluxes, and the typically high wind speeds (Kolstad, 2017), CAO air masses pick up substantial amounts of moisture via evaporation from the ocean surface, which for intense and large-scale CAOs can exceed 5% of the hemispheric water content poleward of 40°N and are, thus, an important element of the high-latitude atmospheric water budget (Aemisegger & Papritz, 2018; Papritz & Sodemann, 2018). Consequently, CAO air masses are rapidly transformed from anomalously cold and dry into much warmer and moist air masses. This can lead to vigorous convective overturning and the release of latent heat during cloud formation (see review by Pithan et al., 2018, and references therein). At the same time, the surface heat fluxes cool the ocean's mixed layer; in fact, CAOs deliver the bulk of the wintertime heat flux forcing of the Nordic Seas (Papritz & Spengler, 2017) and are the key driver for ocean convection at the northernmost extremity of the Atlantic Meridional Overturning Circulation (Buckley & Marshall, 2016; Marshall & Schott, 1999). Due to their important role

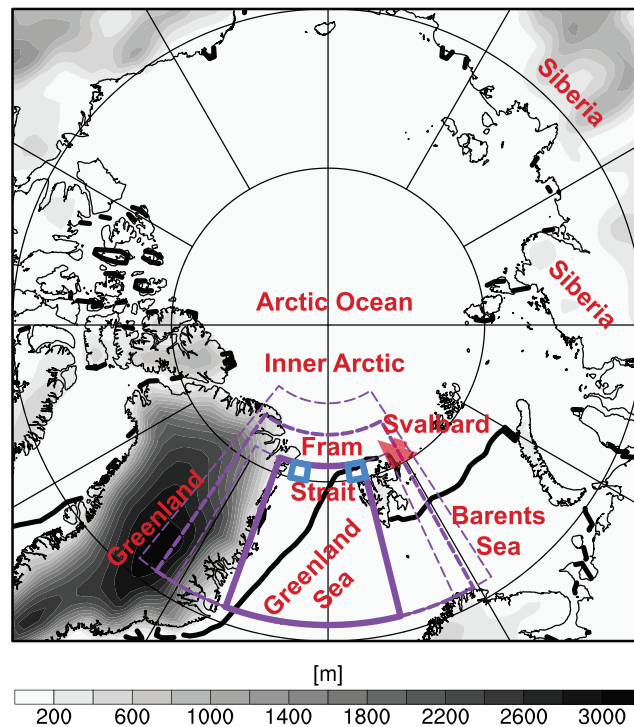


**Figure 1.** Topography in ERA-Interim, winter mean sea ice edge (50% sea ice concentration; black solid), and location names. The purple solid box indicates the region over which the cold air outbreak index is averaged and purple dashed boxes outline standard (thick), shrunk and enlarged (thin) target regions for the tropopause polar vortex tracks (cf. section 4.3). Blue boxes show the regions over which averages of sea level pressure are taken for the computation of the pressure difference over Fram Strait.

in the climate system, CAOs in the Nordic Seas have garnered increasing interest in recent years and—as we outline below—substantial progress has been made in terms of the mechanistic understanding of CAO formation in this region and the associated air mass transformations. Nevertheless, many facets of the drivers of CAO variability remain unexplored and require further investigation.

Climatological analyses revealed that the bulk of the air masses associated with CAOs south of Fram Strait, namely, in the Greenland and Iceland Seas, have their origin in the inner Arctic and are carried through Fram Strait by northerly winds (Kolstad et al., 2009; Papritz & Spengler, 2017). These winds are typically in near geostrophic balance and are, therefore, associated with higher pressure toward northeastern Greenland and lower pressure toward the Svalbard Archipelago (Tsukernik et al., 2009). Consequently, the variability of CAO formation is to a large extent modulated by the frequency of transient cyclones in the Nordic Seas and the Barents Sea. Since Fram Strait is located far north of the primary centers of action of the North Atlantic Oscillation (NAO), and because the North Atlantic storm track features a secondary branch that extends across the Nordic Seas into the Barents Sea (Dacre & Gray, 2009), the flow over Fram Strait exhibits variations that are relatively independent from the NAO (Hilmer & Jung, 2000; Jahnke-Bornemann & Brümmer, 2009). Not surprisingly, this is also reflected in a rather weak correlation between the NAO and CAO occurrence in this region (Kolstad et al., 2009) and a broader spectrum of variability patterns needs to be considered. Papritz and Grams (2018) showed that low-frequency regimes of the midtropospheric large-scale flow that are dominated by either anomalously anticyclonic flow over Greenland or the central North Atlantic, or a trough over Scandinavia, are most conducive for CAO formation. They attributed this relationship to the preferential shift of cyclone activity toward the Norwegian coast and the Barents Sea during these flow regimes, favoring episodes of northerly flow over Fram Strait.

While, as outlined above, the link between the large-scale flow variability and CAO formation from Fram Strait is well studied, it is clear that the availability of sufficiently cold air masses in the inner Arctic is an important prerequisite for intense CAOs. In order to appreciate the full spectrum of CAO variability, one must, therefore, also consider variations in the preconditioning of air masses in the inner Arctic.

The budget of the cold near-surface air mass in the inner Arctic is governed by two opposing processes (Iwasaki et al., 2014). On one hand, the cold air mass is depleted by the episodic and vigorous export of cold air to lower latitudes during CAOs and the subsequent warming of these Arctic air masses due to surface sensible heat fluxes and the release of latent heat. On the other hand, cold air is continuously replenished by longwave radiative cooling. These two processes operate on different timescales. Specifically, Papritz and Spengler (2017) found average cooling rates of about 1.2 K/day in the inner Arctic along kinematic backward trajectories from CAO air masses in the Greenland Sea. In comparison, average heating rates amount to more than 9 K/day when the same air masses are exposed to surface fluxes during a CAO. Thus, the recharge of the cold air mass in the Arctic is a much slower process than its depletion, which results in a temporally oscillating behavior of the Arctic cold air mass (Kanno et al., 2015). As noted by Messori et al. (2018), wintertime cold extremes in the inner Arctic are preceded by a strengthening of the cyclonic flow around the Arctic. In such a flow configuration, the Arctic is more sheltered from lower latitudes and the meridional exchange of air masses is reduced. This implies a longer residence time of air masses in the inner Arctic, while at the same time intrusions of warm and humid air masses from lower latitudes occur less frequently. The air masses in the inner Arctic are, consequently, exposed to uninhibited radiative cooling over a prolonged period and can acquire a substantial temperature deficit with respect to climatology. If northerly winds over Fram Strait happen to tap such a reservoir of unusually cold air, it can be expected that the resulting CAO is particularly intense.

In many cases, the accumulation and coherent transport of anomalously cold Arctic air masses that lead to intense CAOs can—as we will explore in this study—be related to an ubiquitous type of dynamical weather system that is unique to the polar regions, so-called tropopause polar vortices (hereafter TPVs). These are subsynoptic cyclonic vortices at the tropopause level with a diameter of typically 1,000 to 1,500 km and a lifetime of weeks to more than a month (Cavallo & Hakim, 2009, 2010). They are dynamically characterized by a positive potential vorticity (PV) anomaly in the Arctic lower stratosphere, associated with a downward bending of the dynamical tropopause often to the 500-hPa level or below, and a dome of anomalously cold tropospheric air underneath the PV anomaly and a warm anomaly aloft in the stratosphere. They are maintained by differential radiative cooling between the relatively humid troposphere and the very dry stratosphere, which is associated with a diabatic generation of PV near the dynamical tropopause and, hence, an amplification of the TPV (Cavallo & Hakim, 2013). When leaving the inner Arctic, TPVs can instigate the genesis of surface cyclones (Hakim, 2000; Kew et al., 2010). In addition, if the track of the TPV leads over a warm ocean surface, the dome of anomalously cold tropospheric air associated with the TPV is likely resulting in a CAO. By gathering radiatively cooled air masses in their lower tropospheric core, they could also play an important role in the long-range transport of CAO air masses and prolonging their residence time in the inner Arctic. As yet, these potential linkages between CAOs from Fram Strait and TPVs have not been systematically explored. Thus, we hypothesize here that TPVs approaching the vicinity of Fram Strait are an important factor in establishing particularly intense CAOs downstream of Fram Strait.

In this study we aim to address the following questions regarding the dynamical mechanisms and the thermodynamic evolution of the air masses leading to the most intense CAOs from Fram Strait:

1. Does the history of air masses that cause intense CAOs share common characteristics such as a more intense diabatic cooling or a longer residence time in the Arctic compared to air masses that do not?
2. When do these air masses become anomalously cold relative to the time when they pass through Fram Strait?
3. What is the relative importance of diabatic preconditioning and transport from climatologically colder regions toward Fram Strait for establishing the necessary cold anomaly?
4. How often are TPVs involved in the export of very cold Arctic air masses and the formation of intense CAOs?

We consider the 100 most intense CAOs from Fram Strait in the ERA-Interim reanalysis, make use of kinematic trajectories from Fram Strait to investigate the thermodynamic history of these CAO air masses, and implement a feature-based identification and tracking of TPVs. The methodology will be outlined in section 2, followed by the detailed case study of an exceptional sequence of CAOs associated with a long-lived TPV in section 3. Section 4 is then devoted to the climatological investigation of the aforementioned questions, followed by concluding remarks in section 5.

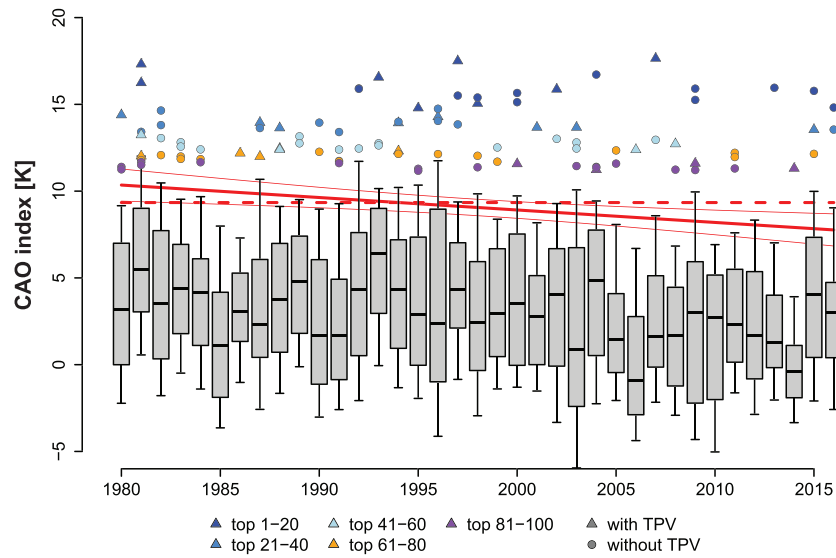


**Figure 2.** Interannual variability of the wintertime 6-hourly CAO index ( $\theta_{\text{SST}} - \theta_{900}$ ) averaged over the Fram Strait box (see Figure 1) with whiskers indicating the 10th to 90th percentile range. The top 100 CAO events with and without TPVs are marked by triangles and circles, respectively. TPV association is evaluated with respect to the standard box (Figure 1). Further shown are the threshold for CAO identification (red dashed) and the linear regression of the seasonal 90th percentile of the CAO index (red solid line). Thin red lines indicate the confidence intervals at the 95% level for the linear regression. CAO = cold air outbreak; TPV = tropopause polar vortex.

## 2. Methodology

We base this study on the interim reanalysis from the European Centre for Medium-Range Weather Forecasts (ERA-Interim; Dee et al., 2011). Fields are available in 6-hourly intervals on 60 model levels, and they are interpolated from the model's spectral T255 resolution onto a regular  $1^\circ \times 1^\circ$  longitude-latitude grid. The study period includes the boreal winters (December–February) 1979/1980 to 2015/2016. Climatological values are defined as the calendar-day climatology, which is the mean over all instances of a specific day of year in the record. For example, the calendar-day climatology for 21 January would be the mean of every 21 January in the record. This time series is then smoothed by a 10-day running mean filter. Thereby, the 10-day running mean provides a reasonable compromise between the desire to retain intraseasonal variations in the climatology and the need to filter out spurious fluctuations resulting from the limited length of the record. In the following, we will introduce three diagnostics that we apply in order to identify principal flow features used for the characterisation of CAOs from Fram Strait. Specifically, these diagnostics comprise (1) the identification of CAO air masses and events, (2) the analysis of transport pathways of air masses reaching Fram Strait from the North, and (3) the identification and tracking of TPVs.

### 2.1. Identification of CAO Air Masses and Events

For the identification of CAO air masses over open ocean we consider the difference between potential sea surface temperature ( $\theta_{\text{SST}}$ ) and  $\theta$  at the 900-hPa level ( $\theta_{\text{SST}} - \theta_{900}$ ). Positive values of this so-called CAO index indicate an air mass colder than the sea surface. Such air masses feature the typical characteristics of marine CAOs, namely, upward fluxes of sensible heat, the uptake of moisture, and convective overturning with cloud formation and the associated release of latent heat (e.g., Brümmer, 1997; Papritz & Sodemann, 2018; Papritz et al., 2015; Renfrew & Moore, 1999). This definition of CAOs has—sometimes with slight variations—been employed in a number of previous studies of CAOs in this region (e.g., Bracegirdle & Gray, 2008; Knudsen et al., 2018; Kolstad & Bracegirdle, 2008; Kolstad et al., 2009; Papritz & Sodemann, 2018; Papritz & Spengler, 2017).

Averaging this CAO index spatially over the region  $20^\circ\text{W}$  to  $14^\circ\text{E}$  and  $71\text{--}81^\circ\text{N}$  (see purple framed box in Figure 1) and excluding grid points over land and over ocean if the sea ice concentration is larger than 0.5 yields the Fram Strait CAO index time series. We identify CAO events in the Greenland Sea as local maxima of this timeseries that exceed its 90th percentile (9.34 K). Start and end dates of a CAO event are then defined as the time steps closest to the first time when the CAO index exceeds or falls below the detection threshold.

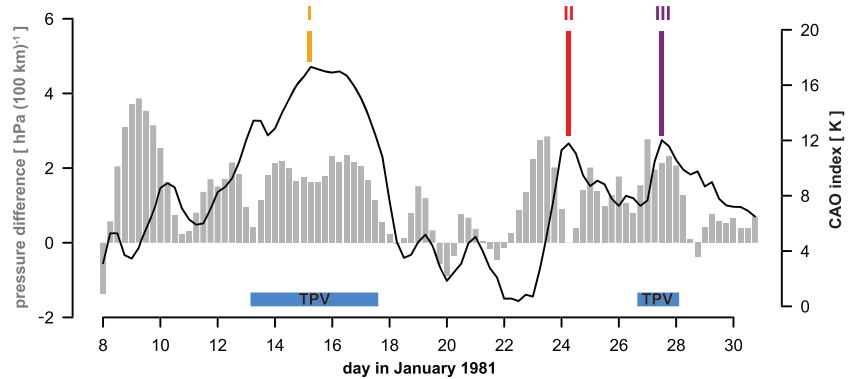


**Figure 3.** Evolution of the CAO index (black;  $\theta_{\text{SST}} - \theta_{900}$ ) averaged over the Fram Strait box (see Figure 1) and the east-west pressure gradient across Fram Strait at 80.5°N (gray bars) from 0000 UTC 8 January to 1800 UTC 30 January 1981. The peaks of the CAO events are marked by I–III, and blue bars indicate the periods during which the TPV track is in the vicinity of Fram Strait (purple, thick dashed box in Figure 1). The CAO index is averaged over the region 20°W to 14°E and 71–81°N (purple, solid box in Figure 1), and the pressure gradient is computed from the difference of sea level pressure averaged over the blue boxes in Figure 1. CAO = cold air outbreak; TPV = tropopause polar vortex.

To avoid the detection of spurious CAO events due to short term fluctuations of the CAO index around the threshold, we treat consecutive CAO events as one single event if less than 20% of the time steps between the onset of the first event and the end of the second event are below the threshold and the time-averaged CAO index exceeds the threshold. Finally, we rank the CAO events according to the maximum of the CAO index reached during the period of each event, in the following referred to as the intensity of the event. This approach results in a total of 146 CAO events throughout the study period, from which we select the 100 most intense events for further analysis (see Figure 2).

Note that the seasonal 90th percentile of the 6-hourly CAO index time series features a declining trend of  $-0.72$  K per decade throughout the study period (Figure 2), which is owed to the more rapid increase of the 900-hPa Arctic air temperature than the SST (not shown). Using a fixed threshold, therefore, may cause the detection of more events at the beginning of the study period than at the end. The pronounced interannual variability of the seasonal 90th percentile, however, clearly dwarves the linear trend (cf. boxplots in Figure 2). Furthermore, the large amplitude of the 100 most intense events compared to the changes in the seasonal 90th percentile implies that all of the events lie outside or at the edge of the confidence interval for the linear regression of the seasonal 90th percentile of the CAO index. Consequently, the same events were detected if the CAO time series was detrended or a threshold linearly decreasing with time was used.

## 2.2. Kinematic Trajectories From Fram Strait

To investigate transport pathways and the thermodynamic evolution of air masses reaching Fram Strait from the inner Arctic, we compute air mass trajectories using the Lagrangian Analysis Tool (LAGRANTO; Sprenger et al., 2015). For that purpose, we define for every 6-hourly time step in the study period a set of points at 900 hPa along the latitude circle of 81.5°N from 20°W to 14°E, that is 0.5° poleward of the northern boundary of the box used for computing the CAO index, with an equidistant horizontal spacing of 35 km, corresponding to twice the longitudinal distance between grid points at 81.5°N. Among these potential trajectory starting points, we select the subset of grid points where the wind has a northerly component. This ensures that trajectories are only computed for air masses that approach Fram Strait from the north. Finally, for these starting points, we compute trajectories forward and backward in time for 48 and 240 hr, respectively, and we trace additional quantities, such as  $\theta$  and the CAO index, by interpolating these fields to the trajectory positions. Throughout the study we will refer to the initialization time of the trajectories as  $t = 0$  hr.

## 2.3. Identification and Tracking of TPVs

As an additional diagnostic, we identify and track TPVs from the anomaly field of PV vertically averaged between 600 and 200 hPa (thereafter referred to as VAPV). Specifically, we define VAPV anomalies as deviations from the calendar-day climatology of VAPV smoothed with a 10-day running mean. The procedure to obtain the TPV tracks involves four steps: First, we identify all local maxima of positive VAPV anomalies poleward of 60°N and search for the outermost closed VAPV anomaly contours surrounding these maxima

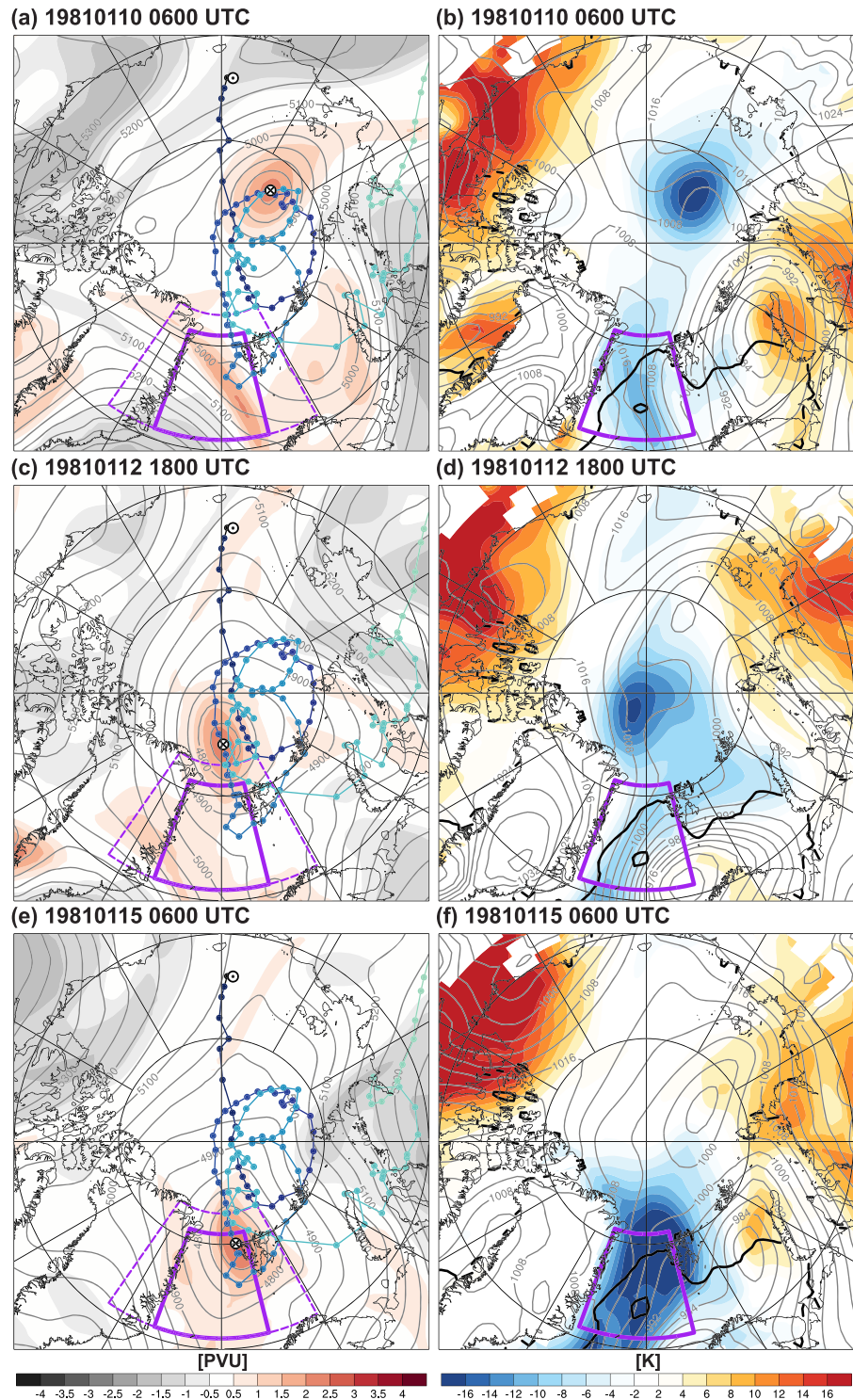


**Figure 4.** Synoptic evolution of CAO event I with peak at 0600 UTC 15 January 1981. Shown are on the left (a, c, e) the VAPV anomaly (shading) and geopotential height at 500 hPa (gray contours; in intervals of 50 m) and on the right (b, d, f) 900-hPa potential temperature anomaly (shading) and sea level pressure (gray contours; in intervals of 4 hPa) at (a, b) 0600 UTC 10 January, (c, d) 1800 UTC 12 January, and (e, f) 0600 UTC 15 January. The left panels additionally show the TPV track (dark blue to light green colors indicating increasing time) with the starting point and the current location of the track indicated by black circles with a dot and a cross, respectively. The sea ice edge (50% sea ice concentration) is indicated on the right by the black solid contour. Purple solid and dashed boxes show the target regions for the CAO index and the TPV track. Meridians are shown at every 30° longitude. CAO = cold air outbreak; TPV = tropopause polar vortex; VAPV = vertically averaged potential vorticity.

with a search interval of 0.1 PVU ( $1 \text{ PVU} = 10^{-6} \text{ K}\cdot\text{kg}^{-1}\cdot\text{m}^2\cdot\text{s}^{-1}$ ). Second, if local maxima occur in close proximity to each other (distance < 800 km), we keep only the largest maximum for further tracking. Third, we employ the tracking algorithm by Wernli and Schwierz (2006) with modifications by Sprenger et al. (2017)—originally developed for the tracking of surface cyclones—to generate tracks of the TPVs. Fourth, we retain only tracks that last for at least 72 hr and attain a VAPV anomaly of 1.5 PVU or more at least once along the track. All in all, this procedure is designed to identify well-defined intense upper tropospheric, cyclonic vortices with a clearly polar origin.

### 3. Case Study of an Episode With Three CAOs

#### 3.1. Synoptic Evolution

In this section, we discuss an episode with a series of three consecutive CAOs that occurred in January 1981, among them the third most intense CAO in the study period. Figure 3 shows the evolution of the CAO index during this period, revealing three distinct peaks, on 15, 24, and 27 January. Thereafter, we will refer to these CAO events as Events I–III. They are ranked 3, 77, and 71 among the 100 CAO events in terms of intensity. A strengthening of the northerly flow precedes these peaks, as evident from the east–west pressure gradient across Fram Strait computed from the difference of area-averaged sea level pressure in the blue boxes shown in Figure 1. This reflects the importance of the transport of cold air masses from the inner Arctic into the basin of the Greenland Sea (cf. Figure 1) for inducing these CAOs (Papritz & Spengler, 2017)—yet the first and most intense CAO is not preceded by exceptionally strong northerly flow compared to the other two events. This suggests that the availability of particularly cold air masses in the inner Arctic is a principal factor in modulating the intensity of CAOs during northerly flow periods.

A unique feature of this episode is the co-occurrence of two of the CAO events with the repeated propagation of a single, long-lived TPV out of the inner Arctic into the vicinity of Fram Strait. The periods when the TPV leaves the inner Arctic near Fram Strait are marked by blue horizontal bars in Figure 3. Furthermore, the synoptic evolution of the episode and the track of the TPV are displayed in Figures 4 and 5. The TPV has genesis north of Bering Strait on 2 January 1981, crosses the North Pole, and then follows a cyclonically curved track, such that it remains in the inner Arctic (cf. track in Figure 4a). At 0600 UTC 10 January the TPV features a cyclonic circulation in the midtroposphere with only a weak signature in surface pressure but a strong negative  $\theta$  anomaly at 900 hPa well exceeding 14 K (Figures 4a and 4b). This  $\theta$  anomaly is clearly linked to the dynamical structure of the TPV, as evident from the vertical cross section shown in Figure 6. It reveals a deep downward excursion of stratospheric air, characterized by PV values in excess of 2 PVU, with the dynamical tropopause (cf. 2-PVU surface) reaching down to about 750 hPa (Figure 6a). Furthermore, it features the archetypal thermal anomalies that are associated with positive PV anomalies (e.g., Hoskins et al., 1985) and a characteristic property of TPVs (Cavallo & Hakim, 2010), which is a cold anomaly underneath the PV anomaly reaching from the surface throughout the entire troposphere and a weaker warm anomaly aloft in the stratosphere (Figure 6b).

Subsequently, the TPV gradually approaches Fram Strait in conjunction with the dome of anomalously cold air underneath, reaching the northern edge of the CAO target region at 1800 UTC 12 January (Figures 4c and 4d). Within the next 2.5 days, the TPV slowly moves further equatorward and thus gives rise to CAO Event I (cf. Figure 3 and Figures 4e and 4f). In this process, the strongly negative  $\theta$  anomaly amplifies substantially as the air masses reach the Greenland Sea—a climatologically much warmer region owing to the relatively warm ocean surface—thus, leading to the strong air–sea temperature contrast.

Eventually, the TPV returns into the inner Arctic and by 1200 UTC 22 January its center is once more located in the vicinity of the North Pole (Figure 5a), while it still maintains a strongly anomalous cold air mass underneath (Figure 5b). Within the next 5 days, it slowly migrates equatorward (Figures 5c and 5d). Thereby, the TPV helps in establishing a cyclonically curved flow that extends beyond the region with anomalously cold air associated with the TPV. This cyclonic flow leads to the transport of cold air masses from Siberia across the central Arctic toward Fram Strait (Figures 5c and 5d). As these air masses approach the climatologically warmer Fram Strait, they attain a negative  $\theta$  anomaly, thus resulting in CAO Event II on 24 January 1981. The TPV itself, however, remains in the inner Arctic.

During the next 4 days, the TPV propagates further equatorward toward Svalbard and then into the Barents Sea. This gives rise to a rapid increase of the CAO index after 0000 UTC 27 January and thus to CAO Event III (Figures 5e and 5f). The resulting  $\theta$  anomaly underneath the TPV is equally strong as during CAO Event

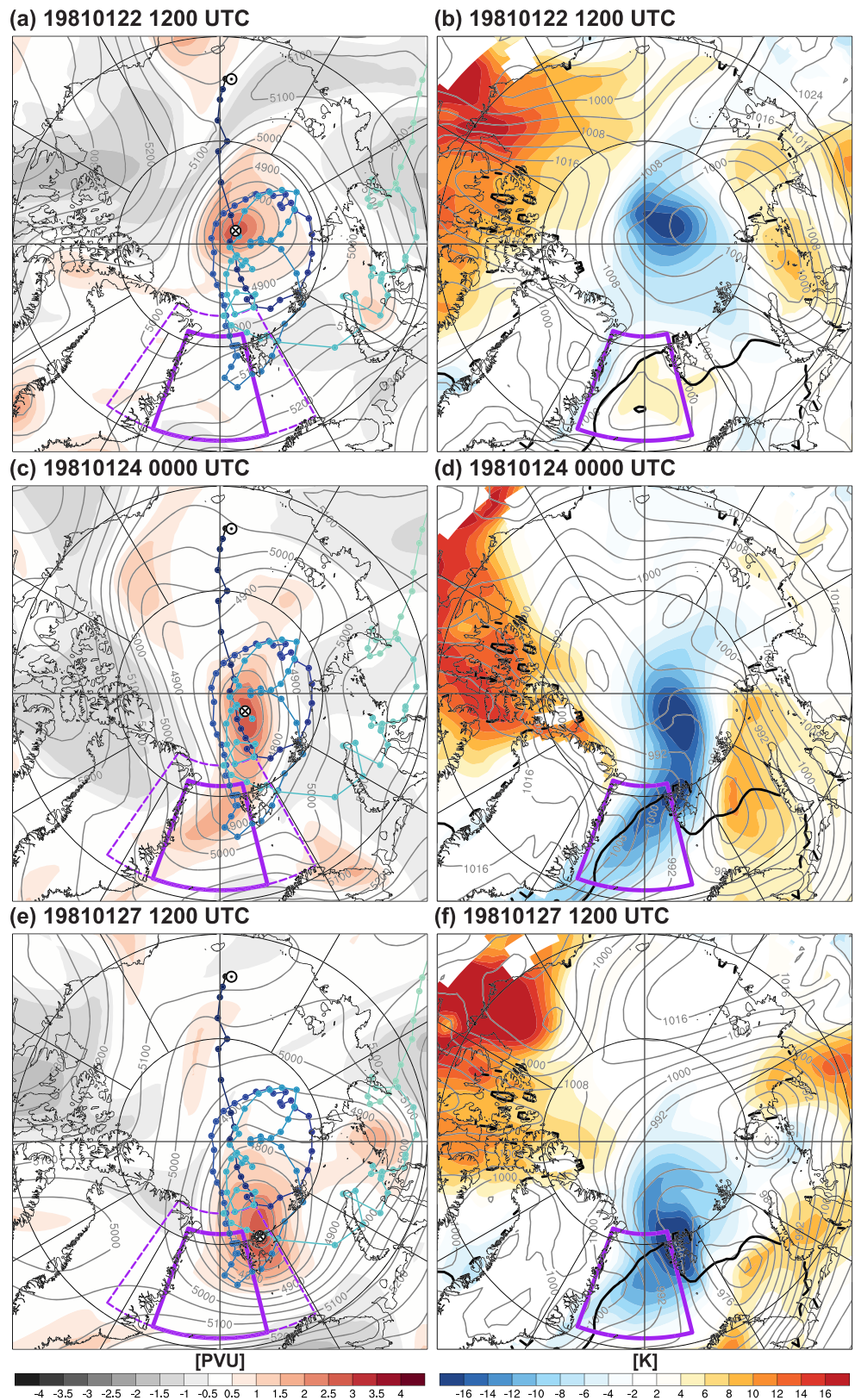


**Figure 5.** As Figure 4 but for cold air outbreak Events II and III with peaks at 0000 UTC 24 January and 1200 UTC 27 January 1981, respectively. Fields are shown at (a, b) 1200 UTC 22 January, (c, d) 0000 UTC 24 January, and (e, f) 1200 UTC 27 January.



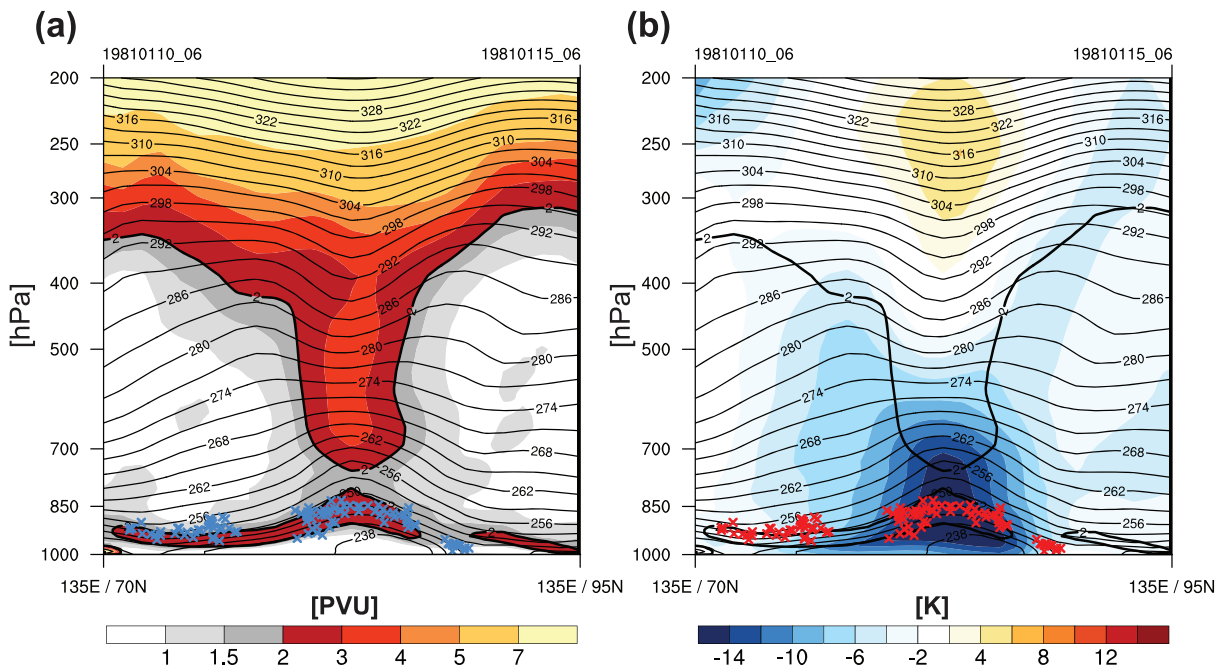


**Figure 6.** Vertical section across tropopause polar vortex (see Figure 7a) at 0600 UTC 10 January 1981 showing (a) potential vorticity and (b) potential temperature anomaly. Further shown are potential temperature (thin black; in intervals of 3 K) and the 2-PVU contour (solid black). Crosses indicate the location of kinematic backward trajectories from Fram Strait released between 24 and 0 hr prior to the peak of Cold Air Outbreak Event I (cf. Figure 7a) and that at 0600 UTC 10 January 1981 have a distance of less than 200 km from the cross section. Note that the different colors of the crosses in (a) and (b) have no meaning and are chosen to maximize visibility.

I (Figures 5d and 5f). Since the track of the TPV is displaced eastward and directed into the Barents Sea, the coldest air masses are located over the Svalbard archipelago and subsequently spill into the Barents Sea, whereas in the Fram Strait region the  $\theta$  anomaly is considerably weaker—yet sufficient to be characterized as an intense CAO. Consequently, the CAO index does not reach as high values as during CAO Event I (Figure 3).

### 3.2. Pathways and Thermodynamic Evolution of CAO Air Masses in the Arctic

Kinematic trajectories from Fram Strait (81.5°N) initialized in 6-hourly intervals from  $-24$  to 0 hr relative to the peak of the CAO event give insight into the transport pathways of the CAO air masses and, in particular, their relation to the TPV. The trajectory locations at the peak times of the CAO events (dots in Figure 7) reveal that trajectories released during this 24-hr period provide a reasonable sampling of the CAO air mass in the CAO target box at the time of maximum intensity. Five days before the peak of CAO Event I, the majority of the trajectories (crosses in Figure 7a) are located in the vicinity of the TPV irrespective of their initialization time. A second group of trajectories are located south of the TPV near the Siberian coast. They are subsequently advected toward Fram Strait by the cyclonic flow in the periphery of the TPV, as exemplified by the explicitly drawn trajectories that were initialized at the peak time of the CAO event. Furthermore, the color shading indicates that all trajectories remained between the surface and about 850 hPa throughout their evolution. The trajectories directly below the TPV have a tendency to descend by about 50–100 hPa until they reach Fram Strait.

The trajectories in the vicinity of the TPV form part of the tropospheric cold dome underneath the TPV as evident from the cross section (crosses in Figure 6b). In fact, most of these trajectories enter the TPV's cold dome already before 7 January more than 8 days before the peak of the CAO event (not shown). Thereafter, these trajectories move in collocation with the TPV. This suggests that the dynamical structure of the TPV provides a material boundary for the anomalously cold air masses allowing for further cooling in accord with an intensification of the TPV (Cavallo & Hakim, 2013). This characteristic is in strong contrast to, for example, extratropical cyclones, where Lagrangian air streams continuously enter and exit the system (e.g., Browning, 1990; Wernli, 1997).

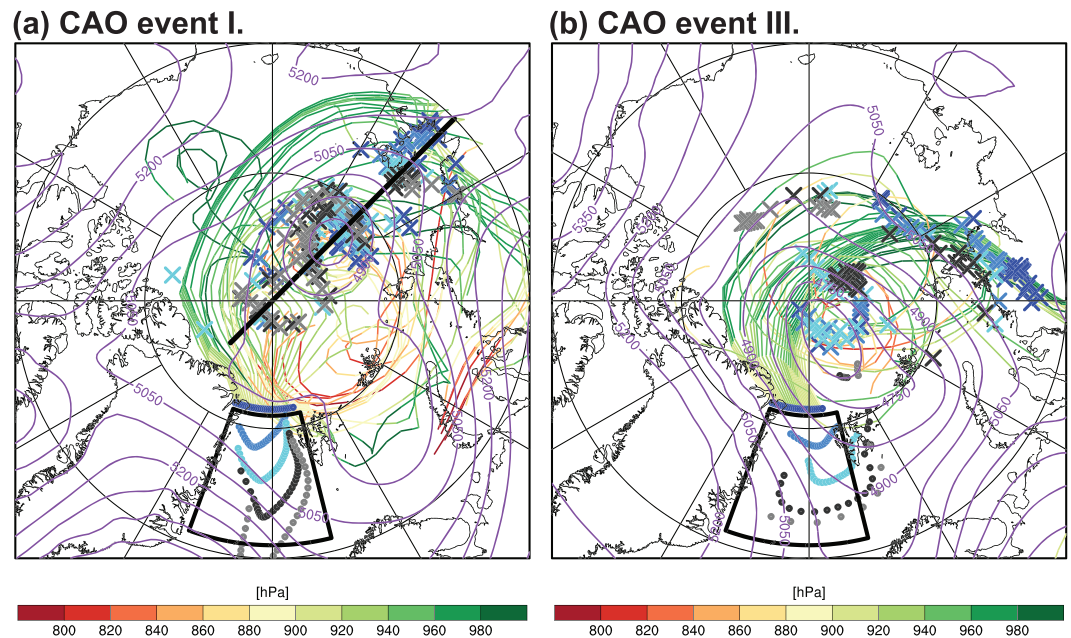


**Figure 7.** Location of cold air outbreak (CAO) air parcel trajectories from Fram Strait contributing to CAO Events (a) I and (b) III. Shown are 500-hPa geopotential height (purple; in intervals of 75 hPa) and the locations of backward trajectories (indicated by X labels) released from Fram Strait 24 hr (light gray), 18 hr (dark gray), 12 hr (cyan), 6 hr (blue), and 0 hr (dark blue) before the peak of the respective event at (a) 0600 UTC 10 January and (b) 0000 UTC 25 January. Additionally shown are trajectory locations at the peak times of the events (dots) and backward trajectories initialized at the peak of the event with colors indicating pressure along the trajectories. The black, solid line in (a) marks the cross section shown in Figure 6, and the black boxes in (a, b) show the CAO target region. Meridians are shown at every 30° longitude.

In the case of CAO Event III a larger group of trajectories reaching Fram Strait originate from Siberia and follows a cyclonically curved pathway across the inner Arctic toward Fram Strait, while only trajectories arriving in the eastern segment of Fram Strait are part of the TPV's cold dome (Figure 7b). Nevertheless, the TPV still plays a key role for the transport of air masses contributing to this CAO event in Fram Strait. Due to the TPV's spatial extent as well as its long residence time near the pole, it gives rise to a near-surface long-range transport from Siberia across the inner Arctic to Fram Strait (cf. trajectories drawn in Figure 7b), which is an important prerequisite for the formation of CAO Event III. A similar long-range transport is also observed for CAO event II (not shown), however, with the TPV remaining in the inner Arctic.

The key factor for the formation of an intense CAO is the existence of a strong  $\theta$  anomaly at the time when trajectories reach Fram Strait (i.e.,  $t = 0$  hr). The relative contributions of transport and diabatic cooling to the emergence of such a  $\theta$  anomaly can be understood in terms of the air masses' distinct signatures in the phase space spanned by  $\theta$  and the climatological  $\theta$  ( $\theta_c$ ; Figure 8). Values in the lower right half of Figure 8 indicate a negative  $\theta$  anomaly. Horizontal displacements from left to right (at constant  $\theta$ ) in this phase space correspond to the creation of a negative  $\theta$  anomaly due to adiabatic transport of an air mass from a climatologically colder into a warmer region, whereas vertical displacements from top to bottom (at constant  $\theta_c$ ) are characteristic of the formation of a negative  $\theta$  anomaly due to diabatic cooling. Accordingly, displacements along the diagonal indicate diabatic cooling in concert with transport from a climatologically warmer into a colder region or vice versa.

Figure 8 reveals a steady cooling of the CAO air masses that contribute to Event I at a rate of about 1 K/day throughout the 10 days until they arrive in Fram Strait corresponding to  $t = 0$  hr. A  $\theta$  decrease on the order of 1 K/day is typical for longwave radiative cooling from water vapor in TPVs (Cavallo & Hakim, 2013). The local climatology,  $\theta_c$ , along the trajectories, in contrast, remains nearly constant during that period. This reflects the fact that the air masses are confined to the TPV and, therefore, are continuously located in the inner Arctic, resulting in a strengthening of the  $\theta$  anomaly. Ultimately, the transport of the CAO air masses through Fram Strait into the climatologically much warmer Greenland Sea gives rise to a median  $\theta$  deficit of well above 20 K at  $t = 6$  hr. Once the air masses are over open ocean, surface sensible heat fluxes and latent

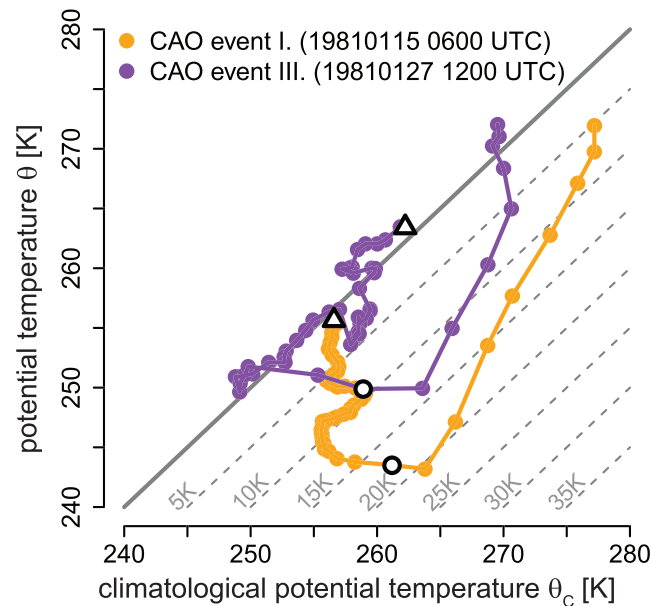


**Figure 8.** Temporal evolution of median potential temperature ( $\theta$ ) versus climatological potential temperature ( $\theta_c$ ) for cold air outbreak (CAO) trajectories initialized during the day before the peaks of CAO Events I and III at 0600 UTC 15 January 1981 (orange) and 1200 UTC 27 January 1981 (purple), respectively. White filled black triangles and circles indicate  $t = -240$  hr and  $t = 0$  hr. Dashed gray lines show negative potential temperature anomaly.

heat release in convection lead to a rapid decline of the temperature deficit and cause an equilibration of the air masses toward the climatological mean  $\theta$  within about 48 hr (Figure 8).

The formation of the negative  $\theta$  anomaly in the case of CAO Event III is strikingly different, even though the air masses are diabatically cooled at a similar rate as those of CAO Event I before reaching Fram Strait. The air masses involved in CAO Event III do not develop a notable cold anomaly prior to approaching Fram Strait (Figure 8). Since an important fraction of these air masses is not confined to the TPV but is transported from Siberia into the inner Arctic along the outer edge of the TPV,  $\theta_c$  along these trajectories decreases at a rate that happens to be in accord with the actual diabatic cooling prior to Event III. Consequently, the median  $\theta$  anomaly only grows as the air masses approach Fram Strait, leading to an anomaly of 14 K at  $t = 6$  hr.

Based on this case study, we conclude that the advection of a TPV into the vicinity of Fram Strait can modulate the formation of CAOs and their intensity in two ways. On one hand, the dome of anomalously cold air collocated with a TPV leads to a tremendous air-sea temperature contrast when the TPV reaches open ocean (Event I and eastern portion of Fram Strait during Event III). On the other hand, the cyclonic circulation in the vicinity of the TPV itself can lead to the long-range transport of air masses along a cyclonically curved trajectory from northern Siberia via the inner Arctic toward Fram Strait (Event II and western portion of Fram Strait during Event III). While these latter air masses are characterized by a weak temperature anomaly in the inner Arctic, they are still sufficiently associated with a substantial temperature anomaly when advected through Fram Strait into the Greenland Sea.

#### 4. Climatology

In the following, we will quantify climatologically when and how negative  $\theta$  anomalies emerge along the equatorward flow of air masses through Fram Strait and how special this evolution is for air masses associated with CAOs compared to air masses that are not. Then, we will assess the relative importance of transport and diabatic cooling for the formation of a strong negative  $\theta$  anomaly during CAO events. Finally, we will quantify the dynamical association of CAO events with TPVs.

##### 4.1. Thermodynamic Preconditioning of CAO Air Masses

Negative  $\theta$  anomalies can arise due to (i) the adiabatic displacement of an air parcel from a climatologically colder into a warmer region, for example, from the inner Arctic across the sea ice edge over open ocean, or (ii) the transformation of the air mass by diabatic cooling. For characterizing the thermodynamic evolution of

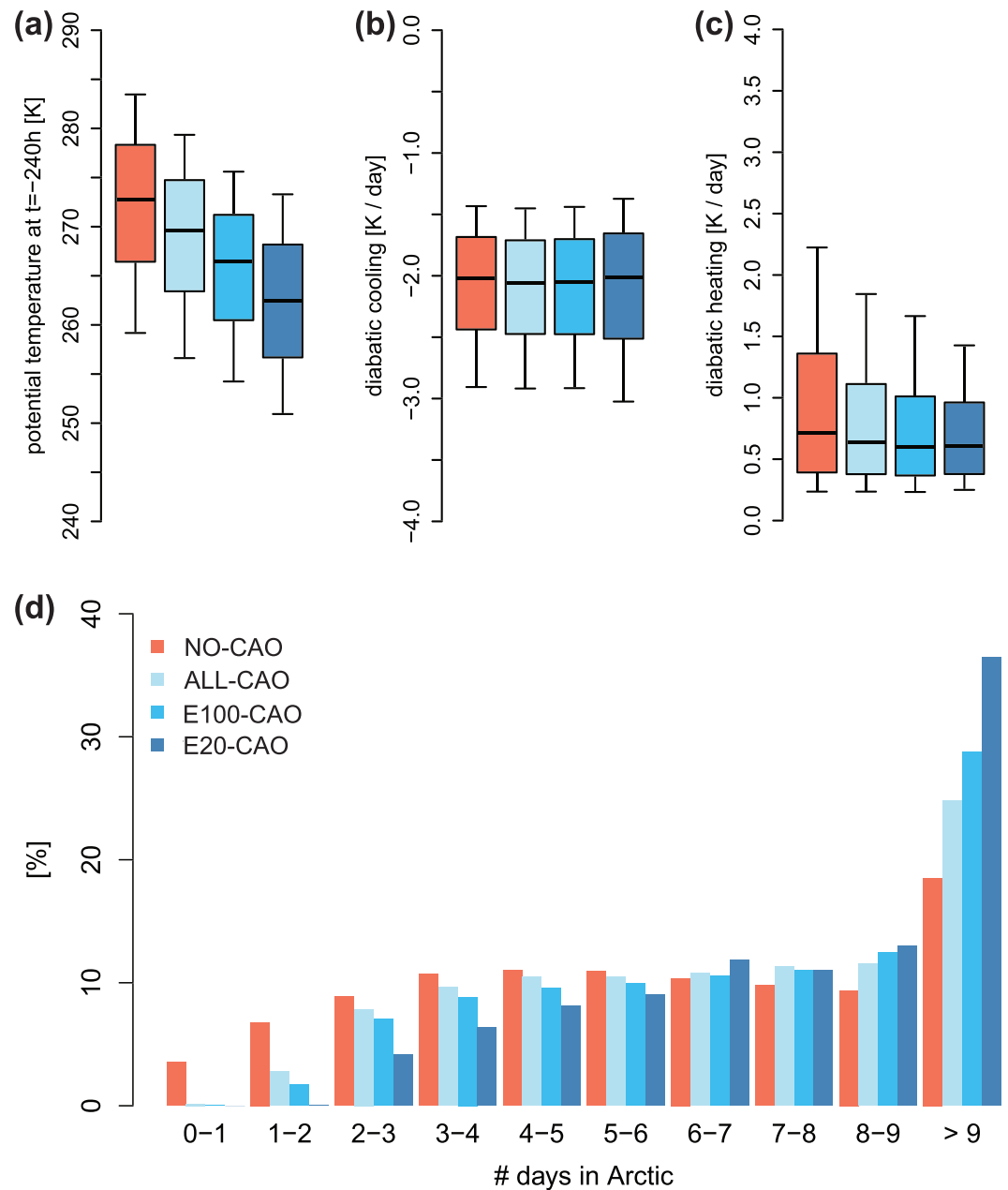


**Figure 9.** Boxplots of (a) potential temperature 10 days prior to arriving in Fram Strait (at  $t = -240$  hr), (b) mean diabatic cooling rate, and (c) mean diabatic heating rate along 10-day backward trajectories from Fram Strait (see text for details). Black lines, boxes, and whiskers denote the median, the interquartile range, and the 10th to 90th percentile range, respectively. (d) Residence time of trajectories in the Arctic (poleward of  $70^\circ\text{N}$  over sea ice or land). Trajectories are grouped into NO-CAO (red), ALL-CAO (light blue), E100-CAO (blue), and E20-CAO (dark blue) trajectories. CAO = cold air outbreak.

air masses and for evaluating the relevance of spatial displacements and diabatic cooling, we consider 10-day backward and 2-day forward trajectories initialized every 6 hr from Fram Strait following the procedure outlined in section 2. We group them into the following four subsets:

1. Trajectories with an air-sea potential temperature difference in excess of the 90th percentile threshold of the CAO index (9.34 K) in the CAO target region ( $20^\circ\text{W}$  to  $14^\circ\text{E}$  and  $71\text{--}81^\circ\text{N}$ ) during at least one 6-hourly time step in the time interval  $0 \leq t \leq 48$  hr after passing Fram Strait (ALL-CAO),
2. as (1) but only for trajectories initialized in Fram Strait during the 24 hr before the time of peak intensity—analogue to the case studies but for all top 100 CAO events (E100-CAO),

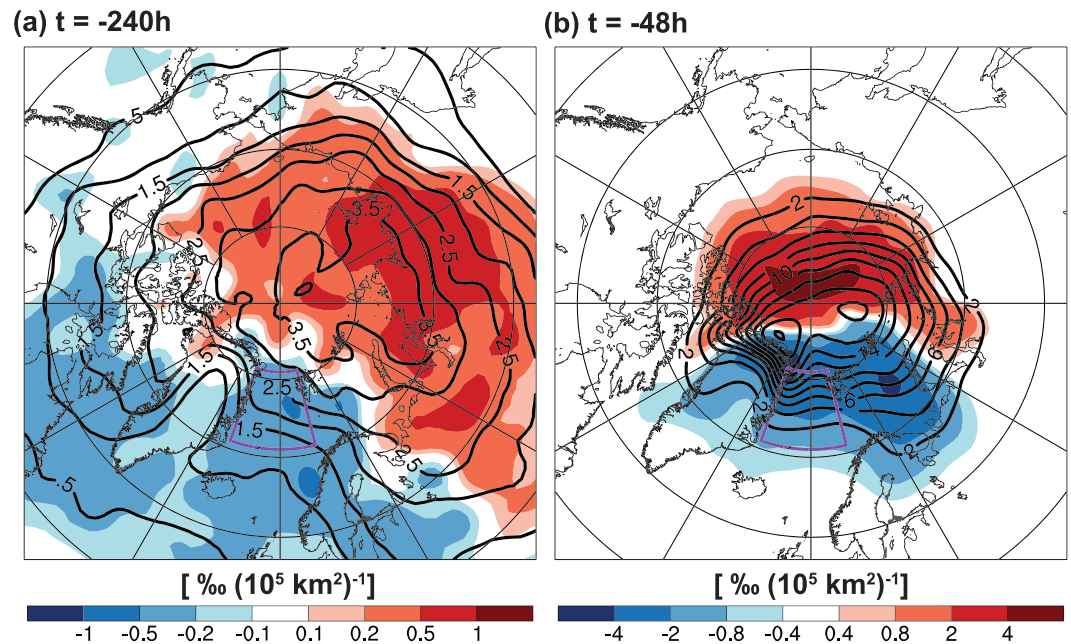


**Figure 10.** Probability for trajectories to be at a certain location (black contours) and difference for ALL-CAO trajectories only with respect to all Fram Strait trajectories (shading) at (a)  $t = -240$  hr and (b)  $t = -48$  hr in units of permille  $(10^5 \text{ km}^2)^{-1}$ . The purple box indicates the CAO target region. Meridians are shown at every  $30^\circ$  longitude. CAO = cold air outbreak.

3. as (2) but for the 20 most intense CAO events only (E20-CAO), and
4. all trajectories not belonging to (1) (NO-CAO).

Note that Groups (1) and (4) are complementary with 34.9% and 65.1% of all trajectories, respectively. Groups (2) and (3) are subsets of (1), comprising 18.3% and 2.9% of ALL-CAO trajectories.

Potential temperature of trajectories at  $t = 0$  hr is determined by their  $\theta$  at  $t = -240$  hr and by the diabatic heating and cooling to which they are exposed along their pathway to Fram Strait. The separate contributions of diabatic heating and cooling to the total change of  $\theta$  along a trajectory are calculated by separately accumulating increments and decrements of  $\theta$  for all 6-hourly trajectory segments (Figure 9). Therefore, for each trajectory the sum of the diabatic cooling and heating rates yields the 10-day net change of  $\theta$ . Ten days before reaching Fram Strait,  $\theta$  of ALL-CAO trajectories is notably lower than that of NO-CAO trajectories (Figure 9a). The distributions of the 10-day average diabatic cooling rates in the two groups of trajectories, however, are nearly identical, which for the median trajectory amounts to about  $-2.0$  K/day (Figure 9b). Also, the medians of the 10-day average diabatic heating rates are similar in each category (Figure 9c), yielding a total  $\theta$  tendency of about  $-1.3$  K/day in close agreement with typical rates found for air masses involved in CAOs in the Greenland Sea (Papritz & Spengler, 2017). Yet 25% of the NO-CAO trajectories also experience diabatic heating of more than 1.4 K/day, which is less for ALL-CAO trajectories with 1.1 K/day. This suggests that ALL-CAO trajectories are for a longer time period shielded from heating processes such as surface sensible heat fluxes than NO-CAO trajectories.

The fact that 10-day average cooling rates across the groups of trajectories are similar may seem like a surprising result. It must be kept in mind, however, that the diabatic cooling is due to the emission of longwave radiation, which is limited by temperature (Boltzmann, 1884; Stefan, 1879) with the emissivity to a large extent controlled by water vapor concentration (see the discussion in Cavallo & Hakim, 2013). Thus, the cooling rate of warmer and moister air masses is likely larger. At the same time, the warmer NO-CAO trajectories experience more frequent episodes dominated by heating than ALL-CAO trajectories, such that in the 10-day average the cooling is about the same for both groups of trajectories. The distinctive feature of ALL-CAO compared to NO-CAO air masses, therefore, must be the residence time in the Arctic during which the air masses are exposed to sustained cooling.

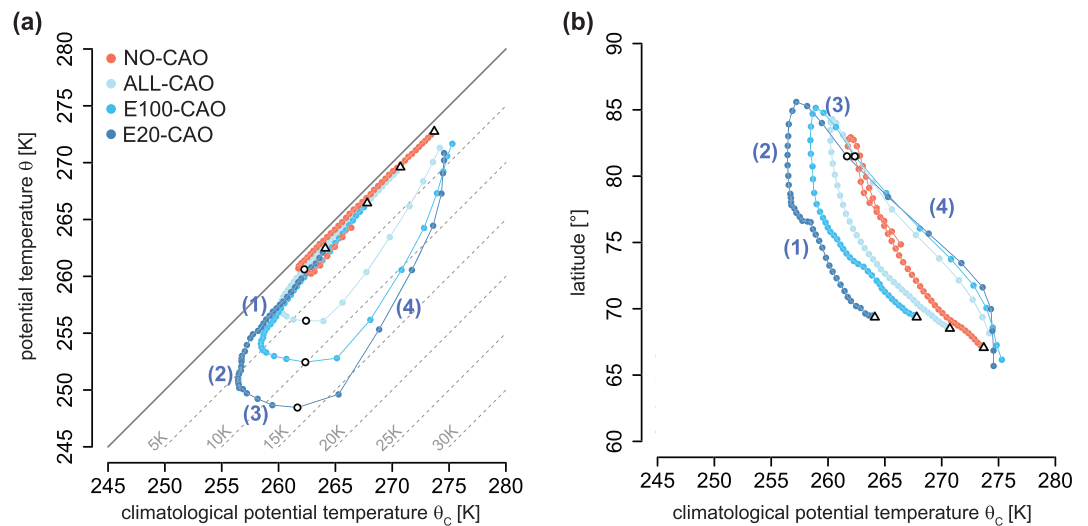


**Figure 11.** Temporal evolution of medians of (a)  $\theta$  versus  $\theta_c$  and (b) latitude versus  $\theta_c$  for Fram Strait trajectories. White filled black triangles and circles indicate  $t = -240$  hr and  $t = 0$  hr, respectively, and colored dots show the medians in 6-hourly intervals. Grouping of trajectories is as in Figure 9. Dashed gray lines in (a) show negative potential temperature anomalies and Labels (1)–(4) indicate the four main phases of trajectory evolution for the E20-CAO category (see text for details). CAO = cold air outbreak.

The above results are substantiated by the residence time of trajectories in the Arctic, which we define as the time period during which the trajectories are continuously located poleward of  $70^\circ\text{N}$  over land or sea ice. This quantifies how long Arctic trajectories are sheltered from intense upward surface sensible heat fluxes, which would rapidly reduce their negative  $\theta$  anomalies. The distribution of the time spent in the Arctic for each group of trajectories clearly shows that ALL-CAO trajectories have a higher Arctic residence time than NO-CAO trajectories (Figure 9d). In addition, 10 days before reaching Fram Strait, ALL-CAO trajectories are more often located over Siberia and in the inner Arctic than NO-CAO trajectories, whereas the latter are more frequently located in the Canadian Arctic, over the Nordic Seas or Scandinavia (Figure 10a). Thus, NO-CAO trajectories are more likely exposed to open ocean and warming by surface sensible heat fluxes, as well as to the uptake of moisture and the consequent release of latent heat on their subsequent pathway to Fram Strait. These systematic differences persist even until 48 hr before arriving in Fram Strait, when the ALL-CAO trajectories are more often located in the inner Arctic near the North Pole than NO-CAO trajectories (Figure 10b).

These differences are even more pronounced when we consider trajectories associated with the 20 most intense CAO events. About 40% of the E20-CAO trajectories spend more than 9 days in the Arctic, whereas this applies to only about 20% of the NO-CAO trajectories (Figure 9d). Furthermore, the former are initially about 10 K colder (Figure 9a) and clearly less than 25% experience diabatic heating of more than 1 K/day (Figure 9c). Hence, we conclude that the lower  $\theta$  of trajectories leading to an intense air-sea temperature difference after passing through Fram Strait is primarily the result of the larger residence time in the inner Arctic, which implies lower  $\theta$  already 10 days prior to the passage through Fram Strait, and a reduced likelihood for the trajectories to be exposed to substantial diabatic heating.

#### 4.2. Relative Importance of Diabatic Cooling and Transport

The differences in the relative importance of diabatic cooling and transport for the formation of a negative  $\theta$  anomaly between the four categories can be summarized in the  $\theta - \theta_c$  phase space (Figure 11a), introduced in section 3.2. Ten days before reaching Fram Strait, the trajectories of all groups are associated with a weak  $\theta$  anomaly; that is, they are close to the diagonal. However, NO-CAO trajectories have about 5 K higher  $\theta$  and  $\theta_c$  values than ALL-CAO trajectories and the subsequent evolution of ALL-CAO trajectories and NO-CAO trajectories follows distinctly different curves in the  $\theta - \theta_c$  phase space. NO-CAO trajectories undergo essentially two phases. First, they are subject to continuous diabatic cooling, and second, as the trajectories approach Fram Strait and pass through it, they are modestly warmed along their equatorward track thereby maintaining a potential temperature close to the local climatology (Figure 11a).

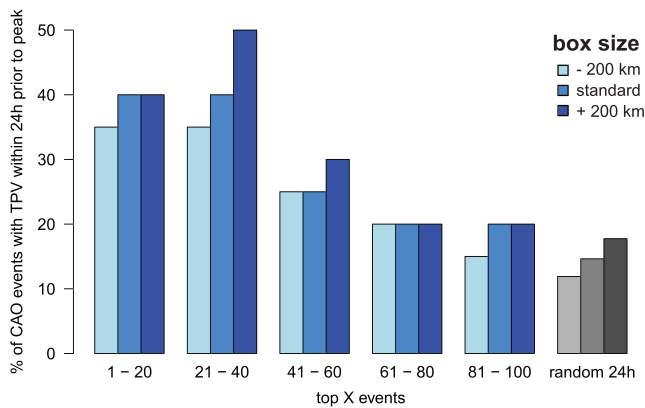


**Figure 12.** Percentage of CAO events sorted by intensity that are associated with a TPV within 24 hr prior to peak of CAO events. The associations are shown for the standard box and for boxes shrunk and enlarged by 200 km in the north-south and west-east directions (leftmost and rightmost bars). See Figure 1 for an outline of the boxes and text for details about the matching procedure. Gray bars denote the frequency of randomly chosen 24-hr intervals that feature a TPV during at least one 6-hourly time step in the respective box. CAO = cold air outbreak; TPV = tropopause polar vortex.

The first phase of ALL-CAO trajectories is analogous to that of NO-CAO trajectories; that is, they are subject to a net diabatic cooling and maintain a weak  $\theta$  anomaly. While starting slightly further poleward and at lower altitude than NO-CAO trajectories (Figure 11b), they reside in regions that are relatively cold for this latitude, consistent with their more frequent location over Siberia than over the North Atlantic (Figure 10a). As they approach the inner Arctic in their second phase, the decrease of  $\theta_c$  stagnates and the diabatic cooling leads to the development of a negative  $\theta$  anomaly. In the third phase, which begins after the trajectories have reached the highest latitude and return equatorward toward Fram Strait,  $\theta_c$  increases jointly with the strong amplification of the  $\theta$  anomaly. Even though the air masses are further cooled diabatically, the strengthening of the  $\theta$  anomaly during that phase is predominantly the result of transport into a climatologically warmer region. The final and fourth phase is characterized by a rapid warming of the air masses due to their exposure to open ocean and the ensuing surface sensible heat fluxes and convective latent heat release. The air masses nearly reach equilibrium with  $\theta_c$  within 48 hr. In this final phase, they are advected to more southerly latitudes with considerably higher  $\theta_c$  than NO-CAO trajectories (Figure 11b).

The trajectories associated with the most intense CAO events undergo a similar four-phase evolution. E20-CAO trajectories reach the northernmost latitude of all groups and are in climatologically colder regions of the Arctic. By the end of the second phase, they have acquired a  $\theta$  anomaly of about 7 K and as they flow toward and through Fram Strait in the third phase, this anomaly amplifies further beyond 15 K mostly due to transport. Thus, the relative importance of the diabatically dominated second phase in comparison to the third transport-dominated phase increases for the most intense CAOs. Major differences are seen in the diabatic warming of the trajectories during the fourth phase. Despite the much stronger negative  $\theta$  anomaly at  $t = 0$  hr, trajectories associated with the most intense CAO events almost reach equilibrium within 48 hr, all at fairly similar  $\theta_c$ . This underlines the efficiency of surface fluxes in the equilibration of anomalously cold air masses over open ocean.

### 4.3. Association With TPVs

Given the key roles of prolonged diabatic cooling (Phase 2) and of coherent transport (Phase 3) for generating the most intense CAO events, as well as the importance of TPVs as dynamical features for the formation of two CAOs during the case study period discussed in section 3, the question arises how often such CAO events are associated with a TPV? To address this question, we select from all identified TPV tracks the subset of tracks affecting Fram Strait based on the following criteria: First, at least one point of the TPV track must be located in the vicinity of Fram Strait (35°W to 29°E/71–83°N; cf. Figure 1). We intentionally choose this region larger than the target box for CAOs, because the center of the TPV may be somewhat displaced from Fram Strait but the TPV nevertheless directly influences the formation of a CAO in the target box (e.g., CAO Event III, Figures 5e and 5f). To test the sensitivity to the choice of the box, we also perform the association of TPVs and CAOs for boxes that are enlarged (shrunk) by 2° latitude to the north and 4° longitude to the west and east (see Figure 1). This results in a variation of the extension of the box of about 200 km in both the north-south and the west-east directions. Second, we require that 60% of the track points are located poleward of 70°N, thus selecting TPV tracks that have spent a major portion of their lifetime at high latitudes. A CAO event is then considered as associated with a TPV if at least one of these TPV tracks is located within the aforementioned region during at least one 6-hourly time step in the 24 hr prior to the peak of the CAO event. Note that with this approach only events where the TPV actually approaches Fram Strait are considered as associated with a TPV (Case Study Events I and III), whereas CAO events where a TPV remains in the inner Arctic are not considered linked to a TPV, even though the circulation associated with a TPV may be relevant for the advection of air masses toward Fram Strait (Case Study Event II). Therefore, the estimates presented here provide a lower bound for the relevance of TPVs for CAO formation.

Among the top 100 CAO events, 29 are associated with a TPV (Figure 2) with an uncertainty of  $\pm 3$  events when the smaller or larger boxes for the association are considered (Figure 12). Considering the trajectories

of CAO events associated with a TPV, we find that they share very similar thermodynamic characteristics as those events with no TPV, albeit with a higher residence time in the inner Arctic (not shown). Nevertheless, there is a strong correlation between the intensity of CAO events and the presence of a TPV. Among the 40 most intense CAO events during the study period, 40% ( $\pm 5\%$ ) are associated with a TPV, while this fraction drops to 20% ( $\pm 2.5\%$ ) for the 40 least intense events (Figure 12). The climatological probability of finding a TPV in the vicinity of Fram Strait during at least one 6-hourly time step in any randomly chosen 24-hr interval is about 14.5% for the standard box (gray bar; Figure 12). This, combined with the relatively small sensitivity to the choice of box, suggests that the association of intense CAO events and TPVs is unlikely an effect of mere chance. Instead, it buttresses the importance of TPVs for inducing many, albeit by far not all, intense CAO events from Fram Strait, reflecting the efficiency of TPVs in gathering anomalously cold air masses and coherently transporting them out of the inner Arctic.

## 5. Discussion and Concluding Remarks

In this study we analyzed the thermodynamic evolution of air masses leading to CAO events south of Fram Strait and we tested the hypothesis that many of the particularly intense CAO events are related to TPVs. In the first part, we presented a detailed case study of an exceptional episode of three intense CAO events that were associated with the repeated passage of a long-lived TPV in the vicinity of Fram Strait. On its way through the Arctic, the TPV intensified and accumulated cold air parcels forming a tropospheric dome with anomalously cold air. As the TPV moved equatorward through Fram Strait and over the open Greenland Sea, it contributed anomalously cold air masses to the third most intense CAO event in the ERA-Interim period. After the TPV's recurvature into the inner Arctic, it maintained a dome of anomalously cold air below it and via its associated cyclonic circulation, it additionally contributed to the long-range transport of air masses from northern Siberia across the inner Arctic toward Fram Strait. This long-range transport and later the passage of the TPV's cold dome over the Svalbard Archipelago gave rise to the second and third CAO events, respectively.

In the second part, we carried out a climatological analysis of the thermodynamic preconditioning of the air masses that contributed to CAOs (ALL-CAO air masses) during winters (December–February) 1979/1980 to 2015/2016. We contrasted their characteristics with those of air masses that were not associated with a CAO (NO-CAO air masses). Specifically, we assessed the Arctic residence time of air masses that pass through Fram Strait as well as the relative roles of transport and diabatic cooling for the presence or absence of an intense negative potential temperature anomaly south of Fram Strait. Finally, using a TPV tracking algorithm, we quantified the association of TPVs and the occurrence of intense CAOs.

Based on the insights from the case study and the climatological analyses, our conclusions with respect to the specific questions raised in section 1 are as follows:

1. CAO air masses differ from NO-CAO air masses in several aspects: 10 days before reaching Fram Strait, CAO air masses are located further poleward or over Siberia—the regions with the lowest climatological  $\theta$  values—and they are colder than NO-CAO air masses. While instantaneous radiative cooling rates are similar for both categories, CAO air masses reside longer in the inner Arctic, thus leading to a larger accumulated diabatic cooling and less episodic warming, for example, due to surface sensible heat fluxes.
2. Until a few days before reaching Fram Strait,  $\theta$  anomalies of CAO and NO-CAO air masses remain weak due to the simultaneous decrease of  $\theta$  and  $\theta_c$  as the air masses are cooled radiatively and move into regions that have climatologically lower potential temperature; that is, they subside or move deeper into the inner Arctic. A notable  $\theta$  anomaly starts to emerge along CAO air masses only about 2 days before reaching Fram Strait as they gradually move equatorward. Only for the air masses contributing to the most intense CAOs (in particular the top 20 CAO events), a strong  $\theta$  anomaly forms already before the air masses start approaching Fram Strait.
3. From the above two findings and the air masses' evolution in the  $\theta - \theta_c$  phase space diagram and the analysis of Arctic residence times, we conclude that the transport of air masses from climatologically colder regions in the Arctic toward Fram Strait is the dominant mechanism for establishing the cold anomaly necessary for the occurrence of a CAO. Enhanced diabatic cooling is of second-order importance for the variability of CAO intensity, whereas an enhanced residence time in the inner Arctic and, thus, a sheltering of the air masses from diabatic heating processes, is key. The air masses that lead to the most intense



CAOs, however, experience a phase where the growth of the  $\theta$  anomaly is dominated by diabatic cooling while the air masses reside in the inner Arctic.

- TPVs are associated with anomalously cold air masses in a low tropospheric cold dome beneath them. The evolution of this cold dome is dynamically linked to the propagation and intensification of the TPV. Based on the TPV tracking we found that in  $29 \pm 3$  of the 100 CAO events analyzed here, the outbreak of the cold air mass is directly linked to the cold dome associated with a TPV in the vicinity of Fram Strait. This TPV-CAO association increases to 40% ( $\pm 5\%$ ) when considering the 40 most intense CAO events, which highlights the importance of TPVs for the efficient formation and coherent transport of anomalously cold air masses.

From these findings it becomes clear that the formation of the most intense CAOs relies on a suitable configuration of the synoptic flow that establishes a transport of air masses from the climatologically coldest parts of the Arctic toward Fram Strait. In this study, the relevance of TPVs for setting up such a transport toward Fram Strait has been emphasized. While TPVs are prevalent in the Arctic (e.g., Hakim & Canavan, 2005), most of them do not leave the inner Arctic near Fram Strait. The underlying dynamical processes that determine if when and where a TPV propagates out of the inner Arctic are not well understood. In particular, it remains unclear whether this is an inherently chaotic process governed, for example, by vortex-vortex interactions in the inner Arctic, or whether also the mutual interaction of TPVs and midlatitude weather systems, such as poleward propagating extratropical cyclones, play an important role. In addition, future studies should explore the validity of this relationship between TPVs and CAOs in other regions known for especially intense CAOs, such as the Labrador Sea and the Ross and Bellingshausen Seas in the Southern Ocean (Kolstad et al., 2009; Papritz et al., 2015).

The intensification and maintenance of TPVs in the Arctic relies on the fact that at cold temperatures typical for the inner Arctic, the moisture content is low such that the contribution of radiative cooling dominates the PV budget near the tropopause over latent heating (Cavallo & Hakim, 2009, 2013). In a warming Arctic, where atmospheric moisture becomes more abundant, TPVs, therefore, may be expected to become less intense. Since many of the most intense CAOs are related to TPVs, as we have shown here, a future warmer climate likely implies an especially pronounced reduction in intensity of the CAOs at the tail-end of the distribution.

#### Acknowledgments

We thank the three anonymous reviewers for their insightful comments that helped to improve the manuscript substantially and the ECMWF for providing access to the ERA-Interim reanalysis. L. P. acknowledges support by the Swiss National Science Foundation (SNSF), Grant P300P2\_174307. The ERA-Interim data underlying this study is available from the website (<http://www.ecmwf.int>).

#### References

- Aemisegger, F., & Papritz, L. (2018). A climatology of strong large-scale ocean evaporation events. Part I: Identification, global distribution, and associated climate conditions. *Journal of Climate*, *31*, 7287–7312. <https://doi.org/10.1175/JCLI-D-17-0591.1>
- Boltzmann, L. (1884). Ableitung des Stefan'schen Gesetzes, betreffend die Abhängigkeit der Wärmestrahlung von der Temperatur aus der elektromagnetischen Lichttheorie. *Annals of Physics*, *258*, 291–294. <https://doi.org/10.1002/andp.18842580616>
- Bracegirdle, T. J., & Gray, S. L. (2008). An objective climatology of the dynamical forcing of polar lows in the Nordic Seas. *International Journal of Climatology*, *28*, 1903–1919. <https://doi.org/10.1002/joc.1686>
- Browning, K. A. (1990). Organization of clouds and precipitation in extratropical cyclones. In C. W. Newton, & E. O. Holopainen (Eds.), *Extratropical cyclones. The Erik Palmén memorial volume* (pp. 129–153). Boston, USA: American Meteorological Society.
- Brümmer, B. (1997). Boundary layer mass, water, and heat budgets in wintertime cold-air outbreaks from the Arctic sea ice. *Monthly Weather Review*, *125*, 1824–1837. [https://doi.org/10.1175/1520-0493\(1997\)125\\$H\\$1824:BLMWAH\\$2.0.CO;2](https://doi.org/10.1175/1520-0493(1997)125$H$1824:BLMWAH$2.0.CO;2)
- Buckley, M. W., & Marshall, J. (2016). Observations, inferences, and mechanisms of Atlantic Meridional Overturning Circulation variability: A review. *Reviews of Geophysics*, *54*, 5–63. <https://doi.org/10.1002/2015RG000493>
- Cavallo, S. M., & Hakim, G. J. (2009). Potential vorticity diagnosis of a tropopause polar cyclone. *Monthly Weather Review*, *137*, 1358–1371. <https://doi.org/10.1175/2008MWR2670.1>
- Cavallo, S. M., & Hakim, G. J. (2010). Composite structure of tropopause polar cyclones. *Monthly Weather Review*, *138*, 3840–3857. <https://doi.org/10.1175/2010MWR3371.1>
- Cavallo, S. M., & Hakim, G. J. (2013). Physical mechanisms of tropopause polar vortex intensity change. *Journal of the Atmospheric Sciences*, *70*, 3359–3373. <https://doi.org/10.1175/JAS-D-13-088.1>
- Dacre, H. F., & Gray, S. L. (2009). The spatial distribution and evolution characteristics of North Atlantic cyclones. *Monthly Weather Review*, *137*, 99–115. <https://doi.org/10.1175/2008MWR2491.1>
- Dee, D., Uppala, S. M., Simmons, A. J., Berrisford, P., Poli, P., Kobayashi, S., et al. (2011). The ERA-Interim reanalysis: Configuration and performance of the data assimilation system. *Quarterly Journal of the Royal Meteorological Society*, *137*, 553–597. <https://doi.org/10.1002/qj.828>
- Hakim, G. J. (2000). Climatology of coherent structures on the extratropical tropopause. *Monthly Weather Review*, *128*, 385–406.
- Hakim, G. J., & Canavan, A. K. (2005). Observed cyclone-anticyclone tropopause vortex asymmetries. *Journal of the Atmospheric Sciences*, *62*, 231–240. <https://doi.org/10.1175/JAS-3353.1>
- Hilmer, M., & Jung, T. (2000). Evidence for a recent change in the link between the North Atlantic Oscillation and Arctic sea ice export. *Geophysical Research Letters*, *27*, 989–992.
- Hoskins, B. J., McIntyre, M. E., & Robertson, A. W. (1985). On the use and significance of isentropic potential vorticity maps. *Quarterly Journal of the Royal Meteorological Society*, *111*, 877–946. <https://doi.org/10.1002/qj.49711147002>

- Iwasaki, T., Shoji, T., Kanno, Y., Sawada, M., Ujiie, M., & Takaya, K. (2014). Isentropic analysis of polar cold air mass streams in the Northern Hemispheric winter. *Journal of the Atmospheric Sciences*, *71*, 2230–2243. <https://doi.org/10.1175/JAS-D-13-058.1>
- Jahnke-Bornemann, A., & Brümmer, B. (2009). The Iceland-Lofotes pressure difference: Different states of the North Atlantic low-pressure zone. *Tellus A*, *61*, 466–475. <https://doi.org/10.1111/j.1600-0870.2009.00401.x>
- Kanno, Y., Abdillahi, M. R., & Iwasaki, T. (2015). Charge and discharge of polar cold air mass in northern hemispheric winter. *Geophysical Research Letters*, *42*, 7187–7193. <https://doi.org/10.1002/2015GL065626>
- Kew, S. F., Sprenger, M., & Davies, H. C. (2010). Potential vorticity anomalies of the lowermost stratosphere: A 10-yr winter climatology. *Monthly Weather Review*, *138*, 1234–1249. <https://doi.org/10.1175/2009MWR3193.1>
- Knudsen, E. M., Heinold, B., Dahlke, S., Bozem, H., Crewell, S., Heygster, G., et al. (2018). Synoptic development during the ALOUD/PASCAL field campaign near Svalbard in spring 2017. *Atmospheric Chemistry and Physics*, *18*, 17,995–18,022. <https://doi.org/10.5194/acp-18-17995-2018>
- Kolstad, E. W. (2017). Higher ocean wind speeds during marine cold air outbreaks. *Quarterly Journal of the Royal Meteorological Society*, *143*, 2084–2092. <https://doi.org/10.1002/qj.3068>
- Kolstad, E. W., & Bracegirdle, T. J. (2008). Marine cold-air outbreaks in the future: An assessment of IPCC AR4 model results for the Northern Hemisphere. *Climate Dynamics*, *30*, 871–885. <https://doi.org/10.1007/s00382-007-0331-0>
- Kolstad, E. W., Bracegirdle, T. J., & Seierstad, I. A. (2009). Marine cold-air outbreaks in the North Atlantic: Temporal distribution and associations with large-scale atmospheric circulation. *Climate Dynamics*, *33*, 187–197. <https://doi.org/10.1007/s00382-008-0431-5>
- Marshall, J., & Schott, F. (1999). Open-ocean convection: Observations, theory, and models. *Reviews of Geophysics*, *37*, 1–64. <https://doi.org/10.1029/98rg02739>
- Messori, G., Woods, C., & Caballero, R. (2018). On the drivers of wintertime temperature extremes in the high Arctic. *Journal of Climate*, *31*, 1597–1618. <https://doi.org/10.1175/JCLI-D-17-0386.1>
- Papritz, L., & Grams, C. (2018). Linking low-frequency large-scale circulation patterns to cold air outbreak formation in the north-eastern North Atlantic. *Geophysical Research Letters*, *45*, 2542–2553. <https://doi.org/10.1002/2017GL076921>
- Papritz, L., Pfahl, S., Sodemann, H., & Wernli, H. (2015). A climatology of cold air outbreaks and their impact on air-sea heat fluxes in the high-latitude South Pacific. *Journal of Climate*, *28*, 342–364. <https://doi.org/10.1175/JCLI-D-14-00482.1>
- Papritz, L., & Sodemann, H. (2018). Characterizing the local and intense water cycle during a cold air outbreak in the Nordic Seas. *Monthly Weather Review*, *146*, 3567–3588. <https://doi.org/10.1175/MWR-D-18-0172.1>
- Papritz, L., & Spengler, T. (2017). A Lagrangian climatology of wintertime cold air outbreaks in the Irminger and Nordic seas and their role in shaping air-sea heat fluxes. *Journal of Climate*, *30*, 2717–2737. <https://doi.org/10.1175/JCLI-D-16-0605.1>
- Pithan, F., Svensson, G., Caballero, R., Chechin, D., Cronin, T. W., Ekman, A. M. L., et al. (2018). Role of air-mass transformations in exchange between the Arctic and mid-latitudes. *Nature Geoscience*, *11*, 805–812. <https://doi.org/10.1038/s41561-018-0234-1>
- Renfrew, I. A., & Moore, G. W. K. (1999). An extreme cold-air outbreak over the Labrador Sea: Roll vortices and air-sea interaction. *Monthly Weather Review*, *127*, 2379–2394. [https://doi.org/10.1175/1520-0493\(1999\)127\\$2379:AECAOO\\$2.0.CO;2](https://doi.org/10.1175/1520-0493(1999)127$2379:AECAOO$2.0.CO;2)
- Sprenger, M., Fragkoulidis, G., Binder, H., Croci-Maspoli, M., Graf, P., Grams, C. M., et al. (2017). Global climatologies of Eulerian and Lagrangian flow features based on ERA-Interim. *Bulletin of the American Meteorological Society*, *98*, 1739–1748. <https://doi.org/10.1175/BAMS-D-15-00299.2>
- Sprenger, M., Wernli, H., & Geoscientific Model Development (2015). The Lagrangian analysis tool LAGRANTO—Version 2.0, 8, 1893–1943. <https://doi.org/10.5194/gmdd-8-1893-2015>
- Stefan, J. (1879). Über die Beziehung zwischen der Wärmestrahlung und der Temperatur. *Sitzungsberichte der mathematisch-naturwissenschaftlichen Classe der kaiserlichen Akademie der Wissenschaften*, *79*, 391–428.
- Tsukernik, M., Deser, C., Alexander, M., & Tomas, R. (2009). Atmospheric forcing of Fram Strait sea ice export: A closer look. *Climate Dynamics*, *35*, 1349–1360. <https://doi.org/10.1007/s00382-009-0647-z>
- Wacker, U., Jayaraman Potty, K. V., Lüpkes, C., Hartmann, J., & Raschendorfer, M. (2005). A case study on a polar cold air outbreak over Fram Strait using a mesoscale weather prediction model. *Boundary-Layer Meteorology*, *117*, 301–336. <https://doi.org/10.1007/s10546-005-2189-1>
- Wernli, H. (1997). A Lagrangian-based analysis of extratropical cyclones. II: A detailed case study. *Quarterly Journal of the Royal Meteorological Society*, *123*, 1677–1706. <https://doi.org/10.1002/qj.49712354211>
- Wernli, H., & Schwierz, C. (2006). Surface cyclones in the ERA-40 dataset (1958–2001). Part I: Novel identification method and global climatology. *Journal of the Atmospheric Sciences*, *63*, 2486–2507. <https://doi.org/10.1175/JAS3766.1>